Sensors and Actuators B 256 (2018) 861–869

Contents lists available at ScienceDirect

Sensors and Actuators B: Chemical

journal homepage: www.elsevier.com/locate/snb

Research paper

# Superior acetone gas sensor based on electrospun $SnO_2$ nanofibers by Rh doping

Xueying Kou, Ning Xie, Fang Chen, Tianshuang Wang, Lanlan Guo, Chong Wang, Qingji Wang, Jian Ma, Yanfeng Sun*, Hong Zhang, Geyu Lu*

*State Key Laboratory on Integrated Optoelectronics, Jilin Province Key Laboratory on Advanced Gas Sensors, College of Electronic Science and Engineering, Jilin University,2699 Qianjin Street, Changchun 130012, People's Republic of China*

ARTICLE INFO

*Article history:*
Received 25 May 2017
Received in revised form 4 September 2017
Accepted 2 October 2017
Available online 5 October 2017

*Keywords:*
Rh-doped $SnO_2$ nanofibers
Electrospinning
Hot pressing
Acetone sensor

ABSTRACT

Undoped and 0.2-1.0 mol% Rh-doped $SnO_2$ nanofibers were fabricated using electrospinning combined with calcination treatment. The fibrous morphology of these nanofibers were maintained and the grain size of the $SnO_2$ nanocrystals were greatly decreased after Rh doping. Sensors based on these nanofibers were fabricated through a hot pressing mathod. The gas sensing properties of these nanofibers were investigated systematically. The results indicated that the response to 50 ppm acetone of 0.5 mol% Rh-doped $SnO_2$ nanofibers was 60.6, which was 9.6 times higher than that of undoped $SnO_2$ nanofibers. In addition, the Rh-doped $SnO_2$ nanofibers showed a decreased cross-response to ethanol, whereas pure $SnO_2$ naofibers did not show selective detection of ethanol and acetone gases. The doping of Rh ions into $SnO_2$ nanocrystals modulates the electron concentration, and induces the changes of the oxygen vacancies and chemisorbed oxygen of $SnO_2$ naofibers. Thus, the doping of $Rh^{3+}$ into $SnO_2$ nanofibers should be a promising method for designing and fabricating acetone gas sensor with high gas sensing performance.



## 1. Introduction

Recently, the research related to gas sensors based on metal oxide semiconductors has attracted continually increasing attention owing to their simplicity of operation, low power consumption and low cost, as well as high sensitivity and extensive application in real-time monitoring of the leakage of poisonous or flammable gases [1–3]. The sensing mechanism of oxide semiconductors gas sensor has been investigated several years and now many researchers support that the interaction between gas molecules and the surface chemisorbed oxygen species is the main reason of the resistance change [4–6]. Take this into consideration, the gas sensing properties of the sensors are closely influenced by the morphology, chemical composition and microstructures of the gas sensing materials [7,8]. As motivated by the driving force of developing oxide semiconductors with enhanced gas sensing performance, great efforts have been adopted on the design of novel types of nanomaterials with elaborate architectures or configurations [9–11]. In the past few decades, researchers have been widely investigated various oxide semiconductors, including ZnO [12–14], $SnO_2$ [15–17], $\alpha$-$Fe_2O_3$ [18–20], NiO [21–23], $WO_3$ [24–26], $In_2O_3$ [27–29] and so on. Tin oxide ($SnO_2$), an *n*-type wide band gap semiconductor (Eg = 3.6 eV at 300 K), has been frequently investigated because of its remarkable properties: high mobility (160 $cm^2/V\,s$) of electrons and high chemical and thermal stability. These properties doubtlessly made $SnO_2$ become a so promising base semiconductor for gas sensor. Based on the fact that the properties of the nanomaterial are strongly dependent on its morphology [30], various methods have been used to synthesize different dimensional and morphological $SnO_2$ nanostructures [31–34]. In addition, it is well-known that the working principle of resistive gas sensor is due to the change of the charge carriers caused by the surface gas-solid interaction. With this in mind, the method of modulating the concentration of charge carriers through aliovalent doping should be an effective way to improve the gas sensing properties [35–38]. Li et al. have provided an evidence of enhanced ethanol response by doping Ni ions on the $SnO_2$ hollow microspheres [39]. Kim et al. have been demonstrated that the response to 5 ppm ethanol could be enhanced up to 15 times via doping $SnO_2$ hollow nanospheres with Pt [40]. Xiao et al.'s work proved that Pd-doped $SnO_2$ performing a high response value of 90–200 ppm ethanol compared with pure $SnO_2$ [41]. These results illustrate that aliovalent doping is an

* Corresponding authors.
*E-mail addresses:* syf@jlu.edu.cn (Y. Sun), lugy@jlu.edu.cn (G. Lu).

https://doi.org/10.1016/j.snb.2017.10.011
0925-4005/

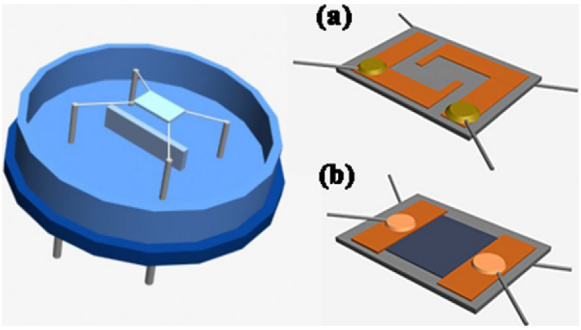


**Fig 1.** Schematic diagram of the gas sensor and the (a) front (b) back of the alumina substrate.

promising approach to modify $SnO_2$ nanomaterial for meliorate its gas sensing performance. Rhodium (Rh) is known as a catalyst in many fields. As for gas sensor, Rh has been used to enhanced both selectivity and sensitivity of the sensing materials to several gases, such as TMA [42], ethanol [43] and so on. However, as far as we know, the reports related to the acetone-sensing performance of Rh-doped $SnO_2$ nanofibers are scarce up to now.

In this work, undoped and various Rh doping amounts of $SnO_2$ nanofibers were synthesized to compare and evaluate the structural features and gas sensing properties. Meanwhile, the optimal Rh doping amount and the effect of $Rh^{3+}$ in the $SnO_2$ nanomaterial on the gas sensing properties were also been examined. As we anticipated, the sensors based on Rh-doped $SnO_2$ nanofibers exhibited improved gas sensing performance to all tested gases. Notablely, the response of the 0.5 mol% Rh-doped $SnO_2$ nanofibers to 50 ppm acetone at 200 °C was 60.6, which was 9.6 times higher than that of undoped $SnO_2$ nanofibers. In addition, the Rh-doped $SnO_2$ nanofibers showed a decreased cross-response to ethanol, whereas pure $SnO_2$ nanofibers did not show selective detection of ethanol and acetone gases. In the end, the role of Rh in the gas sensing mechanism of $SnO_2$ nanofibers was investigated and discussed with respect to its adjustment of the electron concentration, changes of the oxygen vacancies and chemisorbed oxygen of $SnO_2$ nanofibers.

## 2. Experimental section

### 2.1. Synthesis of undoped and Rh-doped $SnO_2$ nanofibers

The undoped and Rh-doped $SnO_2$ nanofibers with various doping concentrations of 0.2, 0.5 and 1.0 mol% were synthesized by electrospinning. Similar to previous synthesis method, the precursor solution for electrospinning was prepared by dissolving 2 mmol $SnCl_2{\cdot}2H_2O$ and a certain dose of $RhCl_3{\cdot}xH_2O$ (0.004 mmol for 0.2 mol%; 0.01 mmol for 0.5 mol%; 0.02 mmol for 1.0 mol%) in a mixture solution containing 5 mL of ethanol and 5 mL of DMF. After magnetic stirring for 30 min at room temperature, 1 g PVP was put in the above mixture solutions with continued stirring for 5 h at 50 °C, until a sticky transparent precursor solution thoroughly formed. After above steps, the precursor solution was moved to a syringe which was connected with a spinneret whose inner diameter was 1.01 mm. The schematic diagram of the usual apparatus for electrospinning had been introduced in our previous work [44]. In electrospinning process, the voltage was 13 kV and the distance between the positive pole (needle) and the negative pole (collector) was 13 cm. The injection speed of the precursor solution was maintained at 0.3 mL/h by using a peristaltic pump. The PVP/$SnCl_2$ or PVP/$SnCl_2$/$RhCl_3$ composite nanofibers mats were obtained after the electrospinning process. The as-synthesized samples were calcined at 500 °C for 2 h in air atmosphere to remove organic polymer components compeletly.

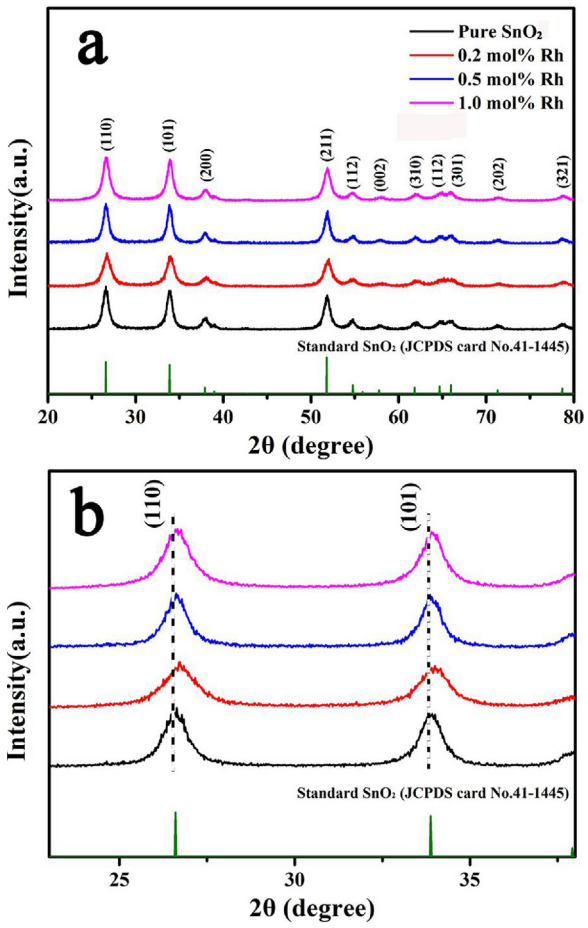


**Fig. 2.** (a) XRD patterns of Rh-doped $SnO_2$ nanofibers with different molar ratios, (b) Comparison of (110) and (101) peaks from XRD patterns.

### 2.2. Characterization

The X-ray diffraction (XRD) patterns were performed through Rigaku TTRIII X-ray diffractometer with Cu Kα radiation at a wavelength of 1.5406 Å at 40 kV and 200 mA. Field emission scanning electron microscopy (FESEM) images were collected by a JEOL JSM-7500F microscope at an acceleration voltage of 15 kV. The energy dispersive X-ray spectroscopy (EDS) spots pattern scanning analysis was recorded by the TEM attachment. Transmission electron microscopic (TEM) and high resolution transmission electron microscopic (HRTEM) images, and selected area electron diffractive (SAED) patterns were acquired on a JEOL JEM-2200FS transmission electron microscope at an operating voltage of 200 kV. The X-ray photoelectron spectroscopy (XPS) measurements were obtained with Mg Kα X-ray source (1253.6 eV Specs XR50).

### 2.3. Fabrication and measurement of gas sensor

The schematic of the fabricated gas sensor is shown in Fig. 1. and the fabrication process is described as follows: the calcined undoped and Rh-doped $SnO_2$ samples were carefully pressed on the alumina substrate (area = 1.0 mm × 1.5 mm, thickness = 0.2 mm), whose diagram is shown in Fig. 1. The alumina substrates were coated with two "L" shape gold electrodes on the front side (electrode widths = 0.3 mm; separation = 0.15 mm) and $RuO_2$ on the back side. The operating temperatures of the sensors were controlled

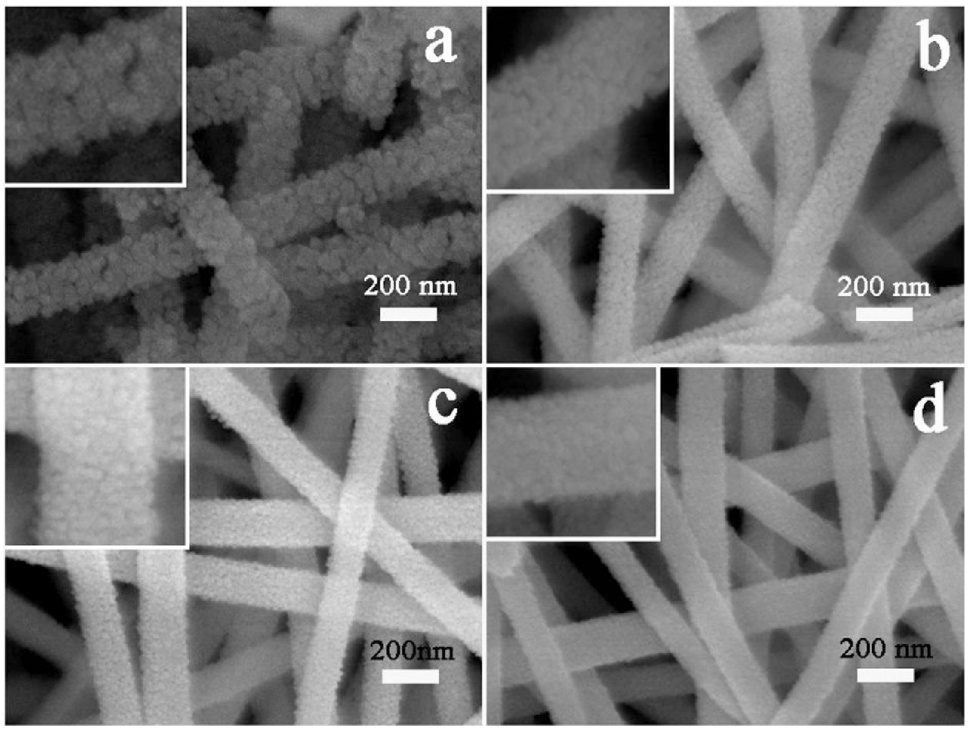


**Fig. 3.** FESEM images of (a) pure (b) 0.2 mol% (c) 0.5 mol% (d) 1.0 mol% Rh-doped $SnO_2$ nanofibers, the insets are high-magnification images.

by the microheater underneath the alumina substrate. The various heater powers corresponding to certain operating temperature value were measured by an FLIR temperature sensor (T250, FLIR Systems Inc., USA). The parameter of hot-press process was fixed to be 120 °C for 5 min. After pressuring the nanomaterials accurately, the nanofibrous mats had a firm adhesion to the alumina substrate. Subsequently, the obtianed sensing device was calcined at 400 °C in air for stabilizing the microstructure of the nanofibers and pre-aging the sensing device effectively. The gas sensing properties of sensors based on undoped and Rh-doped $SnO_2$ nanofibers were tested by a static gas-sensing characterization system, as introduced in the previous works [45]. The gas sensing test of these sensors was under the same condition (RH: 25–35%; temperature: 20–25 °C). According to the definition of gas response, the electrical resistance of the sensor in different environmental atmospheres was measured and the atmospheric air was used as the reference gas. The gas response of the sensors is defined as the ratio of $R_a/R_g$, in which $R_a$ and $R_g$ are the electrical resistance of the sensors in the atmospheric air and target gases. The response and recovery times are defined as the time taken for achieving 90% of the total electrical resistance changes after the sensor was exposed to the atmospheric air and target gases, respectively.

## 3. Results and discussion

### 3.1. Structural and morphological characteristics

The XRD patterns of the undoped and Rh-doped $SnO_2$ nanofibers are shown in Fig. 2a. All of the diffraction peaks could be indexed to tetragonal rutile structure of $SnO_2$, which were agreed well with the recorded values from the Joint Committee on Powder Diffraction Standards card (JCPDS 41–1445). No other phase corresponding to Rh or Rh compound was observed in the XRD patterns of Rh doping samples. In addition, as shown in Fig. 2b, a high angle shift was detected from the (110) and (101) peaks via comparing the Rh-doped $SnO_2$ with pure $SnO_2$. This could be ascribed to the difference between the radii of $Rh^{3+}$ and $Sn^{4+}$. The radius of $Sn^{4+}$ at the coordination number of 6 was 0.690 Å, which was larger than that of $Rh^{3+}$ (0.665 Å) at the same coordination number [46]. Therefore, the substitution of $Sn^{4+}$ by $Rh^{3+}$ induced the high angle shift of diffraction peaks, confirming that $Rh^{3+}$ was incorporated into the $SnO_2$ lattice. Moreover, the average crystallite sizes of the undoped, 0.2 mol%, 0.5 mol% and 1.0 mol% Rh-doped $SnO_2$ samples calculated by Scherrer formula were about 9.85, 7.92, 6.56, and 4.41 nm, respectively, which indicated that the addition of Rh could effectively prevent $SnO_2$ crystallites from further growing up.

Fig. 3a-d shows FESEM images of undoped and 0.2-1.0 mol% Rh-doped $SnO_2$ nanofibers after calcination at 500 °C. All the samples exhibited fibrous nanocrystalline morphology with a uniform diameter about 150 nm. The net structures of nanofibers were observed from all the samples, which were advantageous for the gas to easily diffuse from the surface to the internal of sensing materials. The insets of Fig. 3a-d shows these porous nanofibers were composed of a lot of small nanoparticles and with the Rh doping mount increased, these nanoparticles became smaller. It also could be observed that the grain boundary became more and more indistinct and the nanofibers became more tight. The decrease of grain size indicated that the Rh doping could effectively restrain the growth of $SnO_2$ nanoparticles, which was consistent with the results of XRD.

To further explore the internal structure of these nanofibers, TEM combined with HRTEM and EDS were performed. The TEM images of undoped and 0.5 mol% Rh-doped $SnO_2$ nanofibers in Fig. 4a and Fig. 4d show that the size and morphologies were identical to the images of FESEM. In addition, the porous fibrillar morphology of these nanofibers looks more clear in Fig. 4b and Fig. 4e. The HRTEM images and SAED patterns of the samples indicate that the $SnO_2$ nanofibers were composed of highly crystalline nanoparticles and polycrystalline in nature (Fig. 4c, f). The lattice fringes could be clearly observed in the insets of Fig. 4c, f and the lattice spacings were 0.334 nm, corresponding to the (100) planes of $SnO_2$. For the 0.5 mol% Rh-doped $SnO_2$ samples, the morphology of the nanostructures was maintained after Rh doping, but

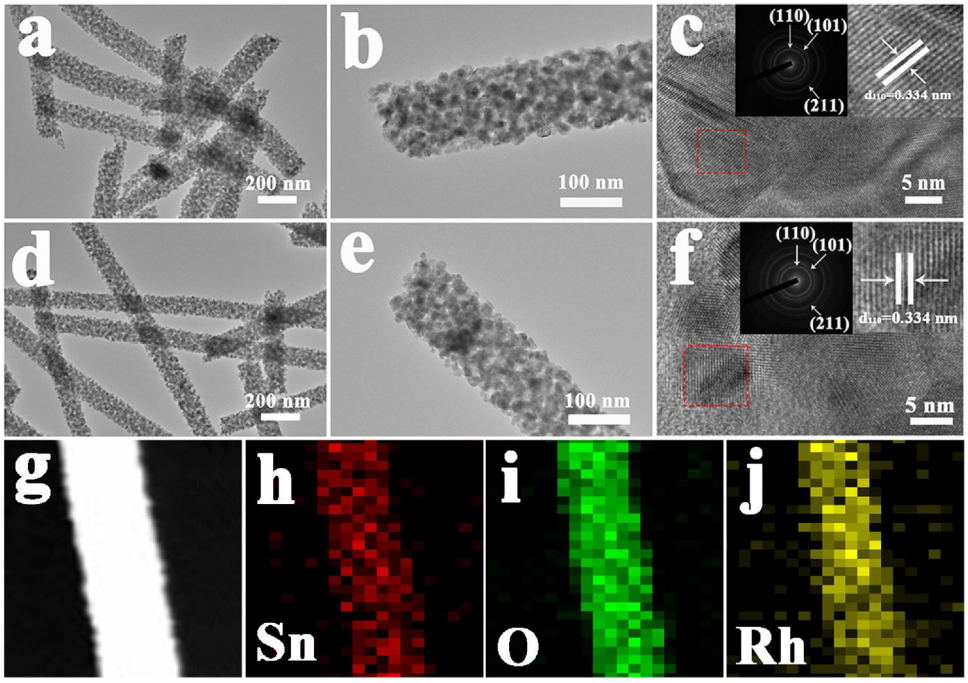


**Fig. 4.** TEM images of (a-c) pure $SnO_2$ naofibers, (d-f) 0.5 mol% Rh-doped $SnO_2$ nanofibers, and (g-j) EDS elemental mapping images of Sn, Rh and O in 0.5 mol% Rh-doped $SnO_2$ nanofibers.

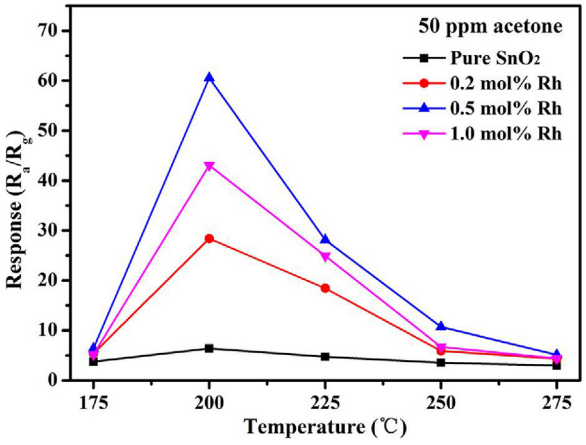


**Fig. 5.** Response of sensors based on pure and 0.2, 0.5, 1.0 mol% Rh-doped $SnO_2$ nanofibers to 50 ppm acetone as a function of the operating temperature.

the nanoparticles which consisted of nanofibers became smaller, as evidenced from TEM and HRTEM images shown in Fig. 4d-f. This was also proved by the results of XRD and FESEM. The EDS elemental mapping images (Fig. 4g-j) indicate these nanofibers were constructed by Rh-doped $SnO_2$ nanoparticles.

In order to confirm that doping of Rh into $SnO_2$ nanofibers is an effective method to enhance the gas sensing properties of the $SnO_2$-based gas sensor, the gas sensing test of the sensors based on undoped and different Rh doping amount of $SnO_2$ nanofibers were carried out. It is well known that the operating temperature and the amount of dopant have great influence on the gas sensing properties of gas sensor. First, the gas responses of the sensors based on undoped, 0.2 mol%, 0.5 mol% and 1.0 mol% Rh-doped $SnO_2$ nanofibers to 50 ppm acetone were tested at different operating temperatures from 175 to 275 °C to find the optimal Rh doping amount as well as the relationship between gas response and operating temperature of the sensors, as shown in Fig. 5.

Obviously, the volcano-shaped relation curve between the gas response and the operating temperature was observed for all the samples, and the optimal operating temperature of every sample was 200 °C. Meanwhile, the gas response was greatly improved due to Rh doping. The gas responses of the sensors based on the undoped, 0.2, 0.5 and 1.0 mol% Rh-doped $SnO_2$ to 50 ppm acetone at 200 °C were 6.3, 28.4, 60.6, and 43.1, respectively. The result indicated that the sensors based on 0.5 mol% Rh-doped $SnO_2$ showed the highest response to 50 ppm acetone and the response value was about 9.6 times higher than that of undoped $SnO_2$. Increasing Rh doping amout to 1.0 mol% decreased the maximum response to 50 ppm acetone to 43.06. However, this is still 6.8 times higher than that of the undoped $SnO_2$ sensor.

Then, the dynamic response characteristics of sensors based on the 0.5 mol% Rh-doped $SnO_2$ nanofibers to 50 ppm acetone were tested. It can be seen that sensors showed reversible response to acetone gas in Fig. 6 (a) and (b). Fig. 6 (a) shows the dynamic response of sensors based on 0.5 mol% Rh-doped $SnO_2$ nanofibers to 50 ppm acetone at 200 °C. It exhibited a fast response and recovery process, and the response and recovery time were about 2 s and 64 s, respectively. It is noted that sensors made in our work exhibited excellent gas sensing performance. Fig. 6 (b) presents five reversible cycles of the response curve that confirmed the 0.5 mol% Rh-doped $SnO_2$ nanofibers had an excellent stability and reversibility when alternately exposed to air and acetone gas.

The real-time response curves of sensors based on pure $SnO_2$ and 0.5 mol% Rh-doped $SnO_2$ nanofibers toward different concentrations of acetone at optimal operating temperature are shown in Fig. 7. It is obvious that the corresponding responses of the two sensors increased with the growth of acetone concentration from 1 to 100 ppm, and the response of the sensor based on the 0.5 mol% Rh-doped $SnO_2$ nanofibers was distinctly higher than that of the undoped $SnO_2$ nanofibers to various acetone concentrations. The responses of sensor based on pure $SnO_2$ nanofibers were 1.1, 1.7, 2.3, 3.3, 6.4, 11.6, 12.1–1, 5, 10, 20, 50, 80, 100 ppm acetone, while the responses of sensor based on 0.5 mol% Rh-doped $SnO_2$ nanofibers were 1.4, 2.8, 8.4, 14.3, 36.2, 60.6, 96.3, 133.3–1, 5, 10, 20,

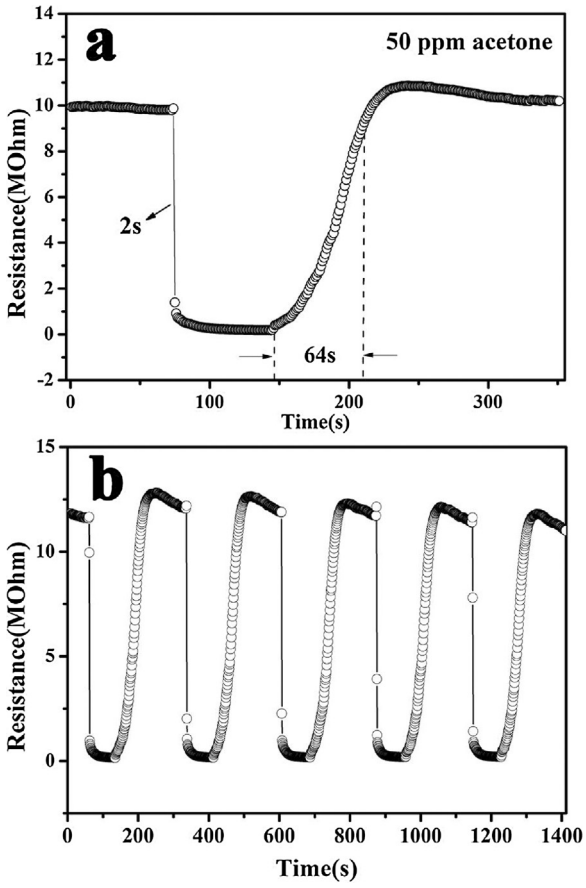


**Fig. 6.** (a) Response and recovery curves (b) Five reversible cycles of sensor based on 0.5 mol% Rh-doped $SnO_2$ nanofibers to 50 ppm acetone at 200 °C.

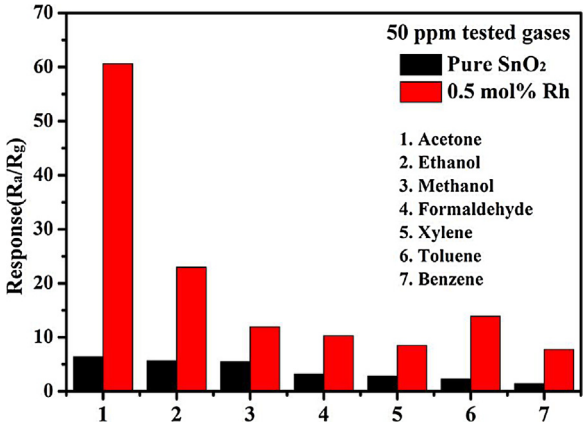


**Fig. 8.** Gas responses of sensors based on pure $SnO_2$ and 0.5 mol% Rh-doped $SnO_2$ nanofibers to 50 ppm various target gases at 200 °C.

50, 80, 100 ppm acetone, respectively. In addition, as shown in the inset of Fig. 7, we could find that the response of the sensor based on the 0.5 mol% Rh-doped $SnO_2$ nanofibers did not tend to saturation gradually when the acetone concentration was raised to 100 ppm. This indicated that the 0.5 mol% Rh-doped $SnO_2$ nanofibers based gas sensor had a broad test range.

Subsequently, the gas responses of sensors based on undoped $SnO_2$ and 0.5 mol% Rh-doped $SnO_2$ nanofibers to 50 ppm of various target gases at 200 °C were tested. As shown in Fig. 8, the response to 50 ppm acetone was greatly enhanced to as high as 60.6 with 0.5 mol% Rh doping, corresponding to a 9.6 times increase at 200 °C. The response to 50 ppm ethanol also showed a higher response ($R_a/R_g = 23$) at 200 °C. It should be noted that Rh doping also increased the ethanol response by 4 times. The responses to methanol ($R_a/R_g = 11.9$), formaldehyde ($R_a/R_g = 10.3$), xylene ($R_a/R_g = 8.5$), toluene ($R_a/R_g = 13.88$), and benzene ($R_a/R_g = 7.75$) were also enhanced substantially by doping with Rh at 200 °C. How-

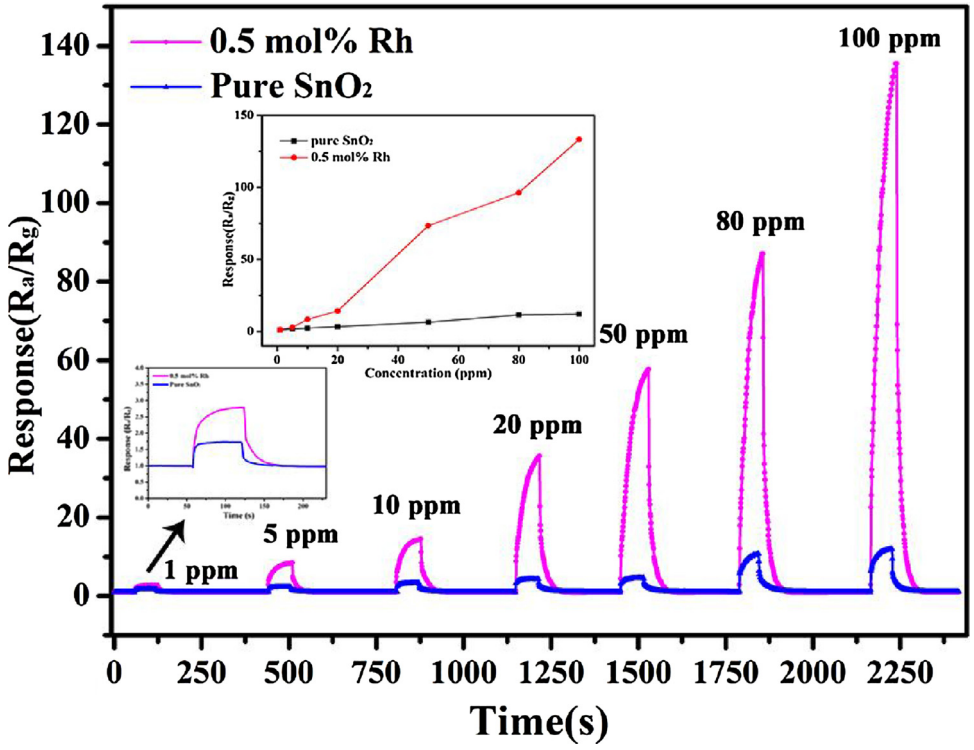


**Fig. 7.** Responses of sensors based on pure $SnO_2$ and 0.5 mol% Rh-doped $SnO_2$ nanofibers versus acetone concentration in the range of 1–100 ppm at 200 °C.

ever, the enhancement of responses to other gases by the doping of Rh was lower than that to acetone gas. Thus, selective detection of acetone can be achieved by using Rh-doped $SnO_2$ nanofibers and it is reasonably that Rh is known as an effective catalyst for selective adsorption of acetone gas [47].

A comparison of the sensing performance between the sensors in this work and other acetone sensors based on $SnO_2$ or some other oxide semiconductor reported previously in the literature are summarized in Table 1 [48–56]. From the table, especially considering the gas response, it is obvious that 0.5 mol% Rh-doped $SnO_2$ nanofibers showed superior gas sensing performance with relatively high gas response. This was beneficial to practical application. Therefore, the sensor based on 0.5 mol% Rh-doped $SnO_2$ nanofibers had more superiority than those reported in the literature.

### 3.2. Mechanism of the enhanced gas sensing performance

It is well-known that the gas sensing performance are greatly influenced by the electrical conductivity and the surface chemisorbed oxygen species of the sensing materials. Thus, the investigations of carrier concentration and distribution of oxygen component in the sensing materials are extremely necessary. First, the resistances in air ($R_a$) were measured to examine the electrical conductivity of the samples (Fig. 9).

We can observe that unlike usual behavior, $R_a$ hardly increased monotonously with lowering the operating temperature. Instead, $R_a$ behaved very uniquely including a region where $R_a$ was almost independent of operating temperature (200 °C–275 °C). This result strongly aligned with the reports in N. Yamazoe's work [57]. It was shown that the unique behavior could be well accounted by electron tunneling transport. In this condition (150 °C–400 °C), the resistance was almost independent of temperature. In addition, another phenomenon was observed that $R_a$ was abnormally increased from 175 °C to 200 °C for all samples. This might be

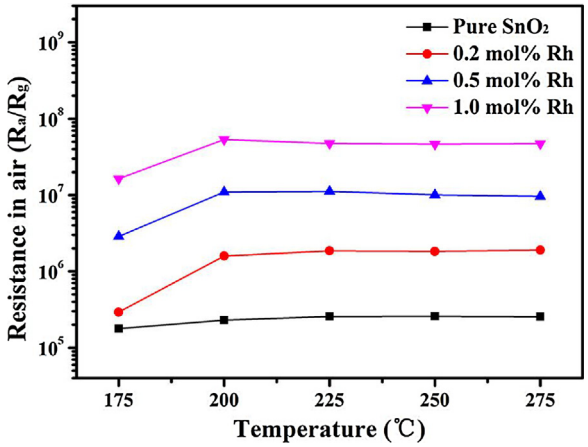


**Fig. 9.** The resistance in air of sensors based on pure $SnO_2$, 0.2, 0.5 and 1.0 mol% Rh-doped $SnO_2$ nanofibers at 175 °C–275 °C.

attributed to the changes of adsorbed oxygen species. The adsorbed oxygen of the surface will be ionized to $O_2^-$ or $O^-$ when the temperature is below 550 °C. More importantly, when the temperature is 200 °C, oxygen adsorbates are changed from $O_2^-$ to $O^-$ species. This process will result in the increase of $R_a$ ($O_2^- + e^- \rightarrow 2O^-$) [58]. So, the value of $R_a$ increased ultimately. Moreover, the $R_a$ of pure $SnO_2$ was 0.23 MΩ at 200 ◦C, while 0.2, 0.5, 1.0 mol% Rh-doped $SnO_2$ showed increased $R_a$ values of 1.59 MΩ, 10.96 MΩ and 53.4 MΩ respectively at the same temperature. The increase of $R_a$ might be explained by the suppression of $SnO_2$ crystallization and the substitute of $Sn^{4+}$ by $Rh^{3+}$. The lower electron concentration of the Rh-doped $SnO_2$ nanofibers could also be understood as their larger Debye length than that of pure $SnO_2$ nanofibers. According to the space charge model of *n*-type semiconductor oxide based

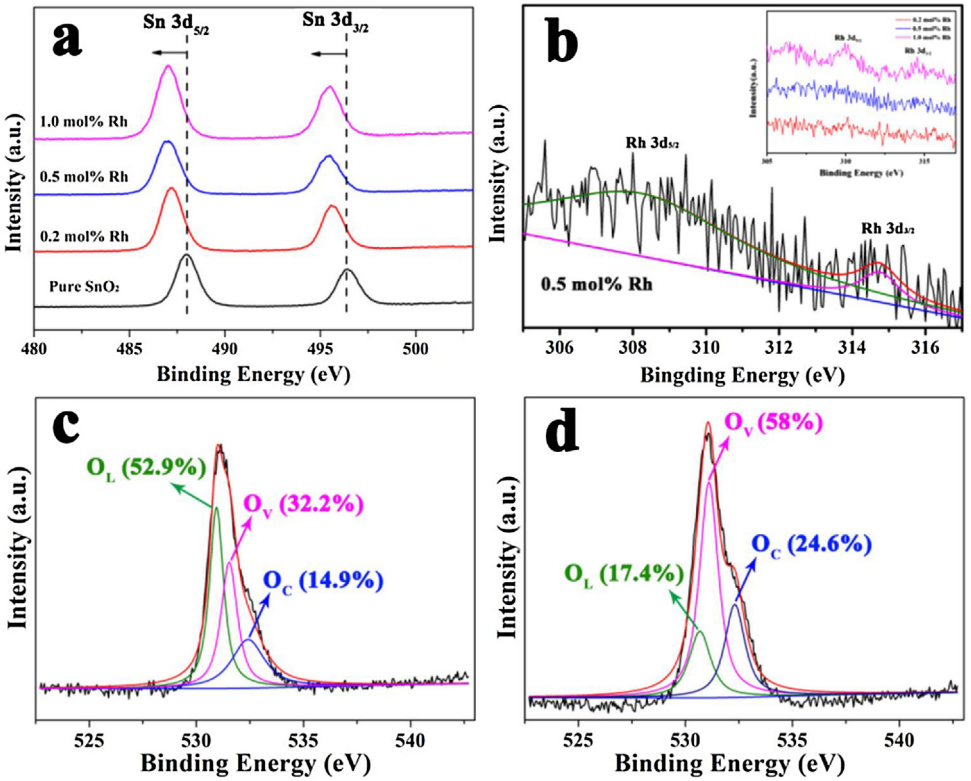


**Fig. 10.** XPS spectra of $SnO_2$ naofibers and Rh-doped $SnO_2$ naofibers. (a) Sn 3d for pure and 0.2-1.0 mol% Rh-doped $SnO_2$, (b) Rh 3d for Rh-doped samples, (c,d) O 1 s XPS spectra of the pure and 0.5 mol% Rh-doped $SnO_2$ naofibers.

**Table 1**
Comparison of the sensing performance between the current work and previously reported results.

| Sensing materials | Acetone Concentration (ppm) | Temperature (°C) | Gas response ($R_a/R_g$) | Ref. |
|---|---|---|---|---|
| $SnO_2$ nanoflowers | 50 | 310 | 11.4 | 42 |
| $SnO_2$ hollow spheres | 50 | 200 | 16 | 43 |
| aurelia-like $SnO_2$ | 50 | 240 | 17 | 44 |
| $SnO_2$ nanoparticles | 200 | 240 | 28.2 | 45 |
| Ce-doped $SnO_2$ hollow spheres | 100 | 250 | 11.9 | 46 |
| NiO-decorated ZnO nanostructures | 100 | 300 | 23.5 | 47 |
| $In_2O_3$ nanoparticles | 100 | 250 | 21.5 | 48 |
| Hollow $\alpha$-$Fe_2O_3$ quasi-cubic structures | 100 | 250 | 8.7 | 49 |
| $In_2O_3$-$WO_3$ nanofibers | 50 | 275 | 12.9 | 50 |
| Rh-doped $SnO_2$ nanofibers | 50 | 200 | 60.6 | This work |

gas sensors, when the grain size was below or equal to twice of the Debye length, the space charge layer of the grain surface could be completely exhausted. Thus, the gas sensing properties could be significantly improved. Second, XPS analysis was performed to further explore the possible mechanism of Rh-doped $SnO_2$ nanofibers (Fig. 10). Fig. 10a presents the high-resolution spectra of Sn 3d and the peaks occured at 488.05 eV and 496.45 eV, which were assigned to Sn $3d_{5/2}$ and Sn $3d_{3/2}$ corresponded to oxidation state +4 of tin atoms ($SnO_2$) [59]. The binding energies of the Sn $3d_{5/2}$ peaks of 0.2-1.0 mol% Rh-doped $SnO_2$ samples (487.25 eV-487.05 eV) were 0.8-1.0 eV lower than that of $SnO_2$ (488.05 eV), indicating the incorporation of $Rh^{3+}$ into the $SnO_2$ lattice. The Rh $3d_{5/2}$ and Rh $3d_{3/2}$ peaks were analyzed using 0.5 mol% Rh-doped samples to identify phase of Rh element at the surface (Fig. 10b). Compared with undoped $SnO_2$, the Rh related peaks were certainly detected and the peaks were observed at the vicinity of $Rh^{3+}$ location (309.45 eV for $3d_{5/2}$, and 314.5 eV for $3d_{3/2}$) [60]. From the inset of Fig. 10b, the intensity of the peak enhanced observably by increasing of Rh amount. In addition, the O 1 s peaks were asymmetric and could be decomposed into three different components [61]. The binding energies were about $529.5 \pm 0.4$ eV ($O_L$), $531.2 \pm 0.6$ eV ($O_V$), and $532.5 \pm 0.2$ eV ($O_C$) corresponding to lattice oxygen, oxygen deficiency, and chemisorbed oxygen species, respectively (Fig. 10c,d). The relative percentages of $O_L$, $O_V$, and $O_C$ components were approximately 52.9%, 32.2%, and 14.9% in the pure $SnO_2$, while they were 17.4%, 58.0%, and 24.6% in the 0.5 mol% Rh-doped $SnO_2$. Obviously, with increasing the Rh doping amount, the contents of $O_V$ and $O_C$ components were greatly increased. It has been reported that the gas sensing properties were closely related to the deficient and chemisorbed oxygen in $SnO_2$ material [62,63]. The increase of $O_V$ component could provide more active sites for the gas reaction and adsorption on the surface of the sensing materials. The increase of $O_C$ component signified that more surface chemisorbed oxygen species could participate in the oxidation-reduction reaction on the surface of the $SnO_2$ nanomaterials and thus resulted in a larger change in the conductivity of sensing materials.

## 4. Conclusion

In summary, undoped and 0.2-1.0 mol% Rh-doped $SnO_2$ nanofibers were synthesized through a simple and facile electrospinning technique. In gas sensing applications, a systematic and comparative analysis indicated that the 0.5 mol% Rh-doped $SnO_2$ nanofibers showed greatly enhanced gas sensing performance, having a response of 60.6–50 ppm acetone at 200 °C, which was 9.6 times higher than that of undoped $SnO_2$ nanofibers. At last, the changes of the electron concentration and distribution of oxygen component induced by the doping of $Rh^{3+}$ into $SnO_2$ nanocrystals were responsible for the enhanced gas sensing performance. Thus, the doping of $Rh^{3+}$ into $SnO_2$ nanofibers should be a promising method for designing and fabricating acetone gas sensor with high performance.

## Acknowledgements

This work was supported by National Nature Science Foundation of China (Nos. 61573164, 61520106003, 61327804). National High-Tech Research and Development Program of China (863 Program, No. 2014AA06A505).

## References

[1] A.C. Romain, J. Nicolas, Long term stability of metal oxide-based gas sensors for e-nose environmental applications: an overview, Sens. Actuators B 146 (2010) 502–506.
[2] X. Zhou, B. Wang, H. Sun, C. Wang, P. Sun, X. Li, X. Hu, G. Lu, Template-free synthesis of hierarchical ZnFe2O4 yolk?shell microspheres for high-sensitivity acetone sensors, Nanoscale 8 (2016) 5446–5458.
[3] G. Korotcenkov, Metal oxides for solid-state gas sensors: what determines our choice? Mater. Sci. Eng. B 139 (2007) 1–23.
[4] Chang-Hoon Kwak, Hyung-Sik Woo, Faissal Abdel-Hady, A.A. Wazzan, Jong-Heun Lee, Vapor-phase growth of urchin-like Mg-doped ZnO nanowire networks and their application to highly sensitive and selective detection of ethanol, Sens. Actuators B 223 (2016) 527–534.
[5] In-Sung Hwang, Joong-Ki Choi, Hyung-Sik Woo, Sun-Jung Kim, Se-Yeon Jung, Tae-Yeon Seong, Il-Doo Kim, Jong-Heun Lee, Facile control of C2H5OH sensing characteristics by decorating discrete Ag nanoclusters on SnO2 nanowire networks, Appl. Mater. Interfaces 3 (2011) 3140–3145.
[6] J. Liu, M. Dai, T. Wang, P. Sun, X. Liang, G. Lu, Kengo Shimanoe, Noboru Yamazoe, Enhanced gas sensing properties of SnO2 hollow spheres decorated with CeO2 nanoparticles heterostructure composite materials, Appl. Mater. Interfaces 8 (2016) 6669–6677.
[7] Tae-Hyung Kim, Ji-Wook Yoon, Yun Chan Kang, Faissal Abdel-Hady, A.A. Wazzan, Jong-Heun Lee, A strategy for ultrasensitive and selective detection of methylamine using p-type Cr2O3: Morphological design of sensing materials, control of charge carrier concentrations, and configurational tuning of Au catalysts, Sens. Actuators B 240 (2017) 1049–1057.
[8] Hyun-Mook Jeong, Jae-Hyeok Kim, Seong-Yong Jeong, Chang-Hoon Kwak, Jong-Heun Lee, Co3O4-SnO2 hollow heteronanostructures: facile control of gas selectivity by compositional tuning of sensing materials via galvanic replacement, Appl. Mater. Interfaces 8 (2016) 7877–7883.
[9] X. Li, X. Zhou, H. Guo, C. Wang, J. Liu, P. Sun, F. Liu, G. Lu, Design of Au@ZnO yolk-shell nanospheres with enhanced gas sensing properties, Appl. Mater. Interfaces 6 (2014) 18661–18667.
[10] Ji-Soo Jang, Sang-Joon Kim, Seon-Jin Choi, Nam-Hoon Kim, Meggie Hakim, Avner Rothschild, Il-Doo Kim, Thin-walled SnO2 nanotubes functionalized with Pt and Au catalysts via the protein templating route and their selective detection of acetone and hydrogen sulfide molecules, Nanoscale 8 (2015) 16417–16426.
[11] Seon-Jin Choi, Saptarshi Chattopadhyay, Jae Jin Kim, Sang-Joon Kim, L. Harry Tuller, C. Gregory Rutledge, Il-Doo Kim, Coaxial electrospinning of WO3 nanotubes functionalized with bio-inspired Pd catalysts and their superior hydrogen sensing performance, Nanoscale 8 (2016) 9159–9166.
[12] X. Xing, T. Chen, Y. Li, D. Deng, X. Xiao, Y. Wang, Flash synthesis of Al-doping macro-/nanoporous ZnO from self-sustained decomposition of Zn-based complex for superior gas-sensing application to n-butanol, Sens. Actuators B 237 (2016) 90–98.
[13] B. Han, X. Liu, X. Xing, N. Chen, X. Xiao, S. Liu, Y. Wang, A high response butanol gas sensor based on ZnO hollow spheres, Sens. Actuators B 237 (2016) 423–430.
[14] S. Li, L. Zhang, M. Zhu, G. Ji, L. Zhao, J. Yin, L. Bie, Acetone sensing of ZnO nanosheets synthesized using room-temperature precipitation, Sens. Actuators B 249 (2017) 611–623.
[15] V. Krivetskiy, I. Malkov, A. Garshev, N. Mordvinova, O.I. Lebedev, S. Dolenko, A. Efitorov, T. Grigoriev, M. Rumyantsev, A. Gaskov, Chemically modified

nanocrystalline SnO2-based materials for nitrogen-containing gases detection using gas sensor array, J. Alloys Compd. 691 (2017) 514–523.
[16] F. Deng, Y. He, G. Shi, B. Li, X. Wu, Low-temperature cataluminescence sensor for sulfur hexafluoride utilizing coral like Zn-doped SnO2 composite, Sens. Actuators B 237 (2016) 120–126.
[17] X. Lian, Y. Li, X. Tong, Y. Zou, X. Liu, D. An, Q. Wang, Synthesis of Ce-doped SnO2 nanoparticles and their acetone gas sensing properties, Appl. Surf. Sci. 407 (2017) 447–455.
[18] X. Guo, J. Zhang, M. Ni, L. Liu, H. Lian, H. Wang, Comparison of gas sensing properties based on hollow and porous α-Fe2O3 nanotubes, J. Mater. Sci.: Mater. Electron. 27 (2016) 11262–11267.
[19] Z. Qiang, S.Y. Ma, H.Y. Jiao, W.X. Jin, T.T. Wang, X.H. Jiang, Z.Y. Zhang, Solvothermal synthesis of 3D leaf-like α-Fe2O3 and its gas-sensing properties research, Mater. Lett. 181 (2016) 29–33.
[20] L. Guo, X. Kou, M. Ding, C. Wang, L. Dong, H. Zhang, C. Feng, Y. Sun, Y. Gao, P. Sun, G. Lu, Reduced graphene oxide/α-Fe2O3 composite nanofibers for application in gas sensors, Sens. Actuators B 244 (2017) 233–242.
[21] Yen-Linh Thi Ngo, Seung Huyn Hur, Low-temperature NO2 gas sensor fabricated with NiO and reduced graphene oxide hybrid structure, Mater. Res. Bull. 84 (2016) 168–176.
[22] Q. Gao, W. Zeng, R. Miao, Synthesis of multifarious hierarchical flower-like NiO and their gas-sensing properties, J. Mater. Sci.: Mater. Electron. 27 (2016) 9410–9416.
[23] Y. Lu, Y.H. Ma, S.Y. Ma, W.X. Jin, S.H. Yan, X.L. Xu, X.H. Jiang, T.T. Wang, H.M. Yang, H. Chen, Z. Qiang, Synthesis of cactus-like NiO nanostructure and their gas-sensing properties, Mater. Lett. 164 (2016) 48–51.
[24] C. Wang, M. Ding, X. Kou, L. Guo, C. Feng, X. Li, H. Zhang, P. Sun, Y. Sun, G. Lu, Detection of nitrogen dioxide down to ppb levels using flower-like tungsten oxide nanostructures under different annealing temperatures, J. Colloid Interface Sci. 483 (2016) 314–320.
[25] Z. Liu, B. Liu, W. Xie, H. Li, R. Zhou, Q. Li, T. Wang, Enhanced selective acetone sensing characteristics based on Co-doped WO3 hierarchical flower-like nanostructures assembled with nanoplates, Sens. Actuators B 235 (2016) 614–621.
[26] K.-H. Kim, S.-J. Kim, H.-J. Cho, N.-H. Kim, J.-S. Jang, S.-J. Choi, I.-D. Kim, WO3 nanofibers functionalized by protein-templated RuO2 nanoparticles as highly sensitive exhaled breath gas sensing layers, Sens. Actuators B 241 (2017) 1276–1282.
[27] F. Huang, W. Yang, F. He, S. Liu, Controlled synthesis of flower-like In2O3 microrods and their highly improved selectivity toward ethanol, Sens. Actuators B 235 (2016) 86–93.
[28] B. Xiao, F. Wang, C. Zhai, P. Wang, C. Xiao, M. Zhang, Facile synthesis of In2O3 nanoparticles for sensing properties at low detection temperature, Sens. Actuators B 235 (2016) 251–257.
[29] S. Zhang, P. Song, J. Zhang, H. Yan, J. Li, Z. Yang, Q. Wang, Highly sensitive detection of acetone using mesoporous In2O3 nanospheres decorated with Au nanoparticles, Sens. Actuators B 242 (2017) 983–993.
[30] C. Wang, J. Liu, Q. Yang, P. Sun, Y. Gao, F. Liu, J. Zheng, G. Lu, Ultrasensitive and low detection limit of acetone gas sensor based on W-doped NiO hierarchical nanostructure, Sens. Actuators B 220 (2015) 59–67.
[31] D. Singh, V.S. Kundu, A.S. Maan, Structural, morphological and gas sensingstudy of palladium doped tin oxide nanoparticles synthesized viahydrothermal technique, J. Mol. Struct. 1100 (2015) 562–569.
[32] C.-H. Kwak, H.-S. Woo, J.-H. Lee, Selective trimethylamine sensors using Cr2O3-decorated SnO2 nanowires, Sens. Actuators B 204 (2014) 231–238.
[33] S. Zhang, P. Zhang, Y. Wang, Y. Ma, J. Zhong, X. Sun, Facile fabrication of awell-ordered porous Cu-doped SnO2 thin film for H2S sensing, ACS Appl. Mater. Interfaces 6 (2014) 14975–14980.
[34] P. Sun, X. Mei, Y. Cai, J. Ma, Y. Sun, X. Liang, F. Liu, G. Lu, Synthesis and gas sensing properties of hierarchical SnO2 nanostructures, Sens. Actuators B 187 (2013) 301–307.
[35] C. Wang, X. Cui, J. Liu, X. Zhou, X. Cheng, P. Sun, X. Hu, X. Li, J. Zheng, G. Lu, Design of superior ethanol gas sensor based on Al-doped NiO nanorod-flowers, ACS Sensors 1 (2016) 131–136.
[36] X. Kou, C. Wang, M. Ding, C. Feng, X. Li, J. Ma, H. Zhang, Y. Sun, G. Lu, Synthesis of Co-doped SnO2 nanofibers and their enhanced gas-sensing properties, Sens. Actuators B 236 (2016) 425–432.
[37] W.X. Jin, S.Y. Ma, Z.Z. Tie, J.J. Wei, J. Luo, X.H. Jiang, T.T. Wang, W.Q. Li, L. Cheng, Y.Z. Mao, One-step synthesis and highly gas-sensing properties of hierarchical Cu-doped SnO2 nanoflowers, Sens. Actuators B 213 (2015) 171–180.
[38] X. Xu, J. Sun, H. Zhang, Z. Wang, B. Dong, T. Jiang, W. Wang, Z. Li, C. Wang, Effects of Al doping on SnO2 nanofibers in hydrogen sensor, Sens. Actuators B 160 (2011) 858–863.
[39] Z. Li, J. Yi, Enhanced ethanol sensing of Ni-doped SnO2 hollow spheres synthesized by a one-pot hydrothermal method, Sens. Actuators B 243 (2017) 96–103.
[40] Bo-Young Kim, Jung Sang Cho, Ji-Wook Yoon, Chan Woong Na, Chul-Soon Lee, Jee Hyun Ahn, Yun Chan Kang, Jong-Heun Lee, Extremely sensitive ethanol sensor using Pt-doped SnO2 hollow nanospheres prepared by Kirkendall diffusion, Sens. Actuators B 234 (2016) 353–360.
[41] L. Xiao, S. Shu, S. Liu, A facile synthesis of Pd-doped SnO2 hollow microcubes with enhanced sensing performance, Sens. Actuators B 221 (2015) 120–126.
[42] Y. Shimizu, Y. Takao, M. Egashira, Detection of freshness of fish by a semiconductive Ru/TiO2 sensor, J. Electrochem. Soc. 135 (1998) 2539–2540.
[43] S.-J. Kim, I.-S. Hwang, C.-W. Na, I.-D. Kim, Y.-C. Kang, J.-H. Lee, Ultrasensitiveand selective C2H5OH sensors using Rh-loaded In2O3 hollow spheres, J. Mater.Chem. 21 (2011) 18560–18567.
[44] C. Feng, X. Li, J. Ma, Y. Sun, C. Wang, P. Sun, J. Zheng, G. Lu, Facile synthesis and gas sensing properties of In2O3-WO3 heterojunction nanofibers, Sens. Actuators B 209 (2015) 622–629.
[45] C. Liu, B. Wang, T. Wang, J. Liu, P. Sun, X. Chuai, G. Lu, Enhanced gas sensing characteristics of the flower-like ZnFe2O4/ZnO, Sens. Actuators B 248 (2017) 902–909.
[46] R.D. Shannon, Revised effective ionic radii and systmatic studies of interatomic distances in halides and chalcogenides, Acta Crystallogr. A 32 (1976) 751–767.
[47] C. Houtman, A. Barteaus, Adsorbed states of acetone and their reactions on Rh (111) and Rh (111)-(2×2) O surfaces, J. Phys. Chem. 95 (1991) 3755–3764.
[48] H. Chen, Q. Wang, C. Kou, Y. Sui, Y. Zeng, F. Du, One-pot synthesis and improved sensing properties of hierarchical flowerlike SnO2 assembled from sheet and ultra-thin rod subunits, Sens. Actuators B 194 (2014) 447–453.
[49] J. Li, P. Tang, J. Zhang, Y. Feng, R. Luo, A. Chen, D. Li, Facile synthesis and acetone sensing performance of hierarchical SnO2 hollow microspheres with controllable size and shell thickness, Ind. Eng. Chem. Res. 55 (2016) 3588–3595.
[50] H. Yu, S. Wang, C. Xiao, B. Xiao, P. Wang, Z. Li, M. Zhang, Enhanced acetone gas sensing properties by aurelia-like SnO2 micro-nanostructures, CrystEngComm 17 (2015) 4316–4324.
[51] L. Li, H. Lin, F. Qu, Synthesis of mesoporous SnO2 nanomaterials with selective gas-sensing properties, J. Sol-Gel Sci. Technol. 67 (2013) 545–555.
[52] P. Song, Q. Wang, Z. Yang, Preparation Characterization and acetone sensing properties of Ce-doped SnO2 hollow spheres, Sens. Actuators B 173 (2012) 839–846.
[53] C. Liu, B. Wang, T. Liu, P. Sun, Y. Gao, F. Liu, G. Lu, Facile synthesis and gas sensing properties of the flower-like NiO-decorated ZnO microstructures, Sens. Actuators B 235 (2016) 294–301.
[54] H. Liu, F. Qu, H. Gong, H. Jiang, M. Yang, Template-free synthesis of In2O3 nanoparticles and their acetone sensing properties, Mater. Lett. 182 (2016) 340–343.
[55] X. Zhou, C. Wang, W. Feng, P. Sun, X. Li, G. Lu, Hollow, α -Fe2O3 quasi-cubic structures: hydrothermal synthesis and gas sensing properties, Mater. Lett. 20 (2014) 5–8.
[56] C. Feng, X. Li, J. Ma, Y. Sun, C. Wang, P. Sun, J. Zheng, G. Lu, Facile synthesis and gas sensing properties of In2O3-WO3 heterojunction nanofibers, Sens. Actuators B 209 (2015) 622–629.
[57] N. Yamazoe, K. Shimanoe, C. Sawada, Contribution of electron tunneling transport in semiconductor gas sensor, Thin Solid Films 515 (2007) 8302–8309.
[58] N. Yamazoe, G. Sakai, K. Shimanoe, Oxide semicomductor gas sensors, Catal. Surv. Asia 7 (2003) 63–75.
[59] J. Zhang, X. Liu, S. Wu, M. Xu, X. Guo, S. Wang, Au nanoparticle-decorated porous SnO2 hollow spheres: a new model for a chemical sensor, J. Mater. Chem. 20 (2010) 6453–6459.
[60] Yoon Ho Cho, Xishuang Liang, Yun Chan Kang, Jong-Heun Lee, Ultrasensitive detection of trimethylamine using Rh-doped SnO2 hollow spheres prepared by ultrasonic spray pyrolysis, Sens. Actuators B 207 (2015) 330–337.
[61] Mohammad R. Alenezi, Abdullah S. Alshammari, K.D.G.I. Jayawardena, Michail J. Beliatis, Simon J. Henley, S.R.P. Silva, Role of the exposed polar facets in the performance of thermally and UV activated ZnO nanostructured gas sensors, J. Phys. Chem. C 117 (2013) 17850–17858.
[62] C. Wang, X. Cui, J. Liu, X. Zhou, X. Cheng, P. Sun, X. Hu, X. Li, J. Zheng, G. Lu, Design of superior ethanol gas sensor based on Al-doped NiO nanorod-flowers, ACS Sensors 1 (2016) 131–136.
[63] L. Gao, F. Ren, Z. Cheng, Y. Zhang, Q. Xiang, J. Xu, Porous corundum-type In2O3 nanoflowers: controllable synthesis, enhanced ethanol-sensing properties and response mechanism, CrystEngComm 17 (2015) 326.

## Biographies

**Xueying Kou** received the B. Eng. degree in department of electronic sciences and technology in 2015. She is currently studying for her M.E. Sci. degree in College of Electronic Science and Engineering, Jilin University, China. Now, she is engaged in the synthesis and characterization of the semiconducting functional materials and gas sensors.

**Ning Xie** received the B. Eng. degree in department of electronic sciences and technology in 2016. Now he is currently studying for degree of master at Jilin University. His work is the synthesis and characterization of the semiconducting functional materials and gas sensors.

**Fang Chen** received her B. Eng. degree from the Electronics Science and Engineering department, Jilin University, China in 2017. Her work is the synthesis and characterization of the semiconducting functional materials and gas sensors.

**Tianshuang Wang** received his B. Eng. degree from the Electronics Science and Engineering department, Jilin University, China in 2015. Presently, he is a graduate student and interested in the synthesis and characterization of the semiconducting functional materials and gas sensors.

**Lanlan Guo** entered her MS course from department of Inorganic Chemistry, Jilin University, China, in 2014. Now, she is studying for her PhD degree, engaged in the synthesis and characterization of the semiconducting functional materials and gas sensors.

**Chong Wang** received the B. Eng. degree in department of electronic sciences and technology in 2013. Now she is currently studying for her PhD degree in College of Electronic Science and Engineering, Jilin University, China.

**Qingji Wang** received the B.E. degree in electronic and information engineering from Beijing University of Chemical Technology in 2007. Now he is a research assistant of Jilin University, China. He is currently studying for his Dr. Eng. degree in College of Electronic Science and Engineering, Jilin University, China.

**Jian Ma** received his MS in 2009 from Jilin University at the Electronics Science and Engineering department. Presently, he is working as Technical Assistant in Electronics Science and Engineering department. His current research interests are gas sensor, the design and fabrication of micro-hot plates.

**Yanfeng Sun** obtained his PhD from Jilin University of China in 2007. Presently, he is working as associate professor in Electronics Science and Engineering department of Jilin University. His current research interests are nanoscience and gas sensors.

**Hong Zhang** obtained her PhD from Jilin University of China in 2008. Presently, she is working as lecturer in Electronics Science and Engineering department of Jilin University. Her current research interests are image processing and sensor technology.

**Geyu Lu** received the BS degree in electronic sciences in 1985 and the MS degree in 1988 from Jilin University in China and the Dr Eng degree in 1998 from Kyushu University in Japan. Now he is a professor of Jilin University, China. Now, he is interested in the development of functional materials and chemical sensors received the B. Eng. Degree in Department of Electronic Science and Technology in 2004. He received his Doctor's degree in College of Electronic Science and Engineering at Jilin University in 2009. Now he is a lecturer of Jilin University, China. His current research is solid electrolyte gas sensor.